

Automatika

Journal for Control, Measurement, Electronics, Computing and Communications



ISSN: (Print) (Online) Journal homepage: <https://www.tandfonline.com/loi/taut20>

Magneto-resistance sensor-based rotor fault detection in induction motor using non-decimated wavelet and streaming data

S. Kavitha, N. S. Bhuvaneshwari, R. Senthilkumar & N. R. Shanker

To cite this article: S. Kavitha, N. S. Bhuvaneshwari, R. Senthilkumar & N. R. Shanker (2022) Magneto-resistance sensor-based rotor fault detection in induction motor using non-decimated wavelet and streaming data, *Automatika*, 63:3, 525-541, DOI: [10.1080/00051144.2022.2052533](https://doi.org/10.1080/00051144.2022.2052533)

To link to this article: <https://doi.org/10.1080/00051144.2022.2052533>



© 2022 The Author(s). Published by Informa UK Limited, trading as Taylor & Francis Group.



Published online: 24 Mar 2022.



Submit your article to this journal [↗](#)



Article views: 493



View related articles [↗](#)



View Crossmark data [↗](#)



Magneto-resistance sensor-based rotor fault detection in induction motor using non-decimated wavelet and streaming data

S. Kavitha^a, N. S. Bhuvaneshwari^b, R. Senthilkumar^a and N. R. Shanker^c

^aElectrical and Electronics Engineering, Saveetha Engineering College, Chennai, Tamil Nadu, India; ^bElectrical and Electronics Engineering, GKM College of Engineering and Technology, Chennai, Tamil Nadu, India; ^cComputer Science and Engineering, Aalim Muhammed Salegh Engineering College, Chennai, Tamil Nadu, India

ABSTRACT

In this paper, the giant magneto-resistance broken rotor (GBR) method is used to diagnose the induction motor (IM) rotor bar fault at an early stage from outward magnetic flux developed by IM. The outward magnetic field signal has anti-clockwise radiation due to broken rotor bar current. In this paper, the outward magnetic signal is acquired using a giant magneto-resistance (GMR) sensor. In the GBR method, IM rotor fault is analysed with a non-decimated wavelet transform (NDWT)-based outward magnetic signal. Experimental result shows the difference in statistical features and energy levels of sub-bands of NDWT for healthy and faulty IM. Least square-support vector machine (LS-SVM)-based classification results are verified by confusion matrix based on 150 outward magnetic signals from a healthy and damaged rotor (broken rotor). The proposed method identifies IM rotor faults with 95% sensitivity, 90% specificity and 92.5% classification accuracy. Furthermore, run-time IM condition monitoring is performed through the ThinkSpeak internet of things (IoT) platform for collecting outer magnetic signal data. ThinkSpeak streaming data of outward magnetic field help detect rotor fault at the initial stage and understand the growth of rotor fault in the motor. The proposed GBR method overcomes sensitivity, translation-invariance limitations of existing IM rotor fault diagnosis methods.

ARTICLE HISTORY

Received 24 January 2021
Accepted 8 March 2022

KEYWORDS

Giant magneto-resistance; broken rotor; rotor fault diagnosis; outward magnetic field; NDWT; IoT

1. Introduction

An induction motor (IM) is an electro-mechanical device used in various industrial applications due to its reliability and robustness. IM has the best robust structure amongst all electrical motors. IM is susceptible to various types of faults, mainly when driven by AC drives [1]. The different faults in IM are bearing fault, stator winding fault, broken rotor bar fault and shaft coupling [2]. According to the IEEE Industrial Application Society (IAS) [3], bearing fault is the major one in small IM, which is comparatively less in large-sized IM. Bearing and stator fault in IM can be minimized by regular maintenance, winding quality, and enhanced design techniques. Hence, a broken rotor bar fault in IM is primarily concerned [4]. The rotor fault is caused by overloading the machine, mechanical cracks and manufacturing defects [5]. The broken rotor bar consumes an excess amount of current flow in the stator and causes an unbalanced magnetic field distribution. This unbalanced magnetic field damages stator winding and raises vibration in IM. Therefore, condition monitoring and fault detection are essential for diagnosing the rotor faults at an early stage in IM, avoiding machine failure and unnecessary shutdown.

IM fault diagnosis methods are classified as signal-based techniques, model-based techniques [6], and knowledge-based techniques. In signal-based

techniques, current, voltage, leakage flux signal parameters are used for fault detection [7]. The motor current signature analysis (MCSA) is the signal-based technique of rotor bar fault diagnosis. Many MCSA-based methods had been implemented for rotor bar fault diagnosis by spectral analysis techniques, such as autoregressive-based spectrum methods [8], wavelet transforms [8], Taylor–Kalman [9], low-frequency and load torque oscillations [10], high-resolution parameter estimation [11]. The above MCSA-based methods can effectively monitor the stator current parameter remotely and identify the faults through signal analysis. However, false fault warning is the major problem in MCSA-based methods [12]. The Multiple Signal Classification (MUSIC) algorithm-based approach is applied widely for IM broken rotor bar fault detection [13]. This method leads over the single-phase signal waveform analysis of rotor fault detection. However, the amplitude of the single-phase current signal is inadequate for detecting the broken rotor fault at an early stage.

Broken rotor bar faults can be diagnosed by vibration signal, temperature monitoring [14,15] and acoustic emission monitoring techniques [16]. The vibration monitoring-based technique requires expensive sensors such as accelerometer, Hall effect sensor, and piezoelectric sensor. The above sensors have major problems in mounting the sensor on IM [17].

Furthermore, the vibration analysis provides the geometry of IM, and control features such as frequency response function [18]. Acoustic emission and temperature monitoring methods require specific Data Acquisition (DQA) Devices for hardware implementation. Acoustic and temperature signals of the motor are influenced by ambient environmental conditions and microclimatic conditions. Hardware complexity and machine geometry are related drawbacks of sensor-based methods and can be eliminated by non-contact methods such as infrared thermography [19] and stray flux analysis [17]. Infrared thermography-based approach uses an infrared camera for detecting the hot spots in IM. However, this method detects little faults in the specific parts of the IM, such as the magnetic circuit insulation issues and deficient connections. Flux measurement based non-contact method uses search coils and probes for fault detection in IM. The search coils and probes are inadequate to capture the total flux around the machine. Therefore, the fault estimation and monitoring are performed approximately.

Several model-based approaches [20–22] are developed to minimize the hardware complexity in IM fault detection and estimation. Model-based methods depend on mathematical modelling for predicting the faults in IM. They can warn and detect the faults in IM; accuracy depends on mathematical concepts in prediction. Hence, knowledge-based methods are preferred; they use artificial intelligence, soft computing algorithms for IM fault detection. The artificial neural network (ANN) is preferred in knowledge-based intelligent methods [23,24] because of its precise pattern recognition ability. Fuzzy logic [25,26] and support vector machines (SVM) [27–30] infer the different stages of rotor faults. Several other soft computing-based approaches, such as principal components analysis (PCA) [31], nearest neighbour (NN) [32] and machine learning [33], are used for rotor fault diagnosis in IM with good sensitivity and specificity. Knowledge-based methods have limitations, such as the requirement of large training data, necessity of retraining, whenever machine specifications change. Hence, condition monitoring and fault detection in IM need an accurate and precise non-contact method with optimized and proper sensor mounting on the motor. Until now, Fourier analysis is the standard method used for diagnosing the rotor faults in IM. However, the performance of Fourier's techniques is constrained by the resolution in signals. To overcome resolution problem, motor signals are analysed by discrete wavelet transform (DWT). However, the classification outcome of DWT-based approach is also inadequate due to the lack of translation-invariance property of DWT. The finite element method (FEM) provides a high-resolution signal. However, FEM-based methods require a longer execution time because of computational complexity. Hence, there is a need for a motor signal analysis method with

a better resolution and translation-invariance ability. Moreover, inferences from the literature survey show that the low sensitivity and inappropriate mounting of the sensor affect the accuracy of IM fault detection. Hence, optimum sensor selection and mounting are prerequisites for accurate fault diagnosis in IM.

To overcome the above problem, we propose the giant magnetoresistance broken rotor (GBR) method for the early detection of rotor faults in IM. The proposed GBR method uses giant magnetoresistance (GMR – NV Electronics-AA002) sensor for measuring outward magnetic field for rotor fault detection. The GMR sensor has a good sensitivity and the optimized location of the sensor on the motor is detected and the maximum amount of outward magnetic signal is captured. The GBR method identifies the rotor condition of IM using the features extracted from the NDWT processed outward magnetic signal spectrum. The GBR method performs NDWT analysis and overcomes the lack of translation-invariance issue of conventional wavelet transform (WT)-based signal analysis. Moreover, the proposed GBR method has an LS-SVM classification algorithm for rotor fault detection. Furthermore, condition monitoring of IM is performed through the internet of things (IoT) using live data acquisition of outward magnetic signals. The major contributions are summarized as below:

- (1) The BR method analyses the outward anti-clockwise magnetic flux signal based on the optimum location of sensor and the distance between the GMR sensor and motor for the maximum acquisition of anti-clockwise outward magnetic flux. The location of the GMR sensor in IM changes according to the size and fabrication of IM and rotor size. Location of IM is detected by the maximum outward magnetic flux signal amplitude. The distance between the GMR sensor and IM varies based on the size of IM. To identify, optimized distance and location to acquire the maximum outward magnetic field signal spectra from IM is about 10 and 20 cm distance. The above distance is between the rotor axis and the GMR sensor. The 10 and 20 cm distance is for the acquisition of minimum and maximum magnetic signals with high intensity.
- (2) To perform, NDWT, DWT, Dyadic, DWT-NDWT and Dyadic-NDWT signal analysis for energy level and statistical features extraction from the outward magnetic field signals, diagnose the rotor fault in IM using a soft computing approach such as LS-SVM and classify the outcome features of the NDWT for rotor fault detection.
- (3) To develop an IoT-based online condition monitoring system for continuous monitoring of the condition of the IM during run-time through live

streaming data of transform processed outward magnetic field signal.


The remainder of this paper is organized as follows: Section 2 describes the latest literature review. The proposed GBR approach of various processing steps such as optimized sensor placement, hybrid wavelet analysis of the outward magnetic spectra, LS-SVM-based IM fault detection, and condition monitoring using IoT is explained in Section 3. The experimental results obtained using the real motor data are given in Section 4 to verify the efficiency of the proposed GBR approach for run-time IM fault detection and condition monitoring. Finally, this paper is concluded in Section 5. This paper focuses on the early detection of IM rotor faults with high sensitivity and specificity. To determine the limitations and requirements in IM rotor fault detection, and a literature review of recent IM rotor fault detection conducted is analysed and summarized in Table 1.

2. Literature survey on recent research in IM rotor fault detection

3. Proposed framework for fault detection and monitoring

The sequential processing steps of the proposed GBR method for IM broken rotor bar fault diagnosis are illustrated in Figure 1. In the GBR method, an outward magnetic field of IM is acquired by the GMR sensor placed at the optimized location of the stator outer region. Location varies according to rotor size and winding of IM. Optimum location of GMR sensor for acquisition of outward magnetic flux is identified through co-efficient energy level and statistical features of magnetic signal from wavelet transform. GMR sensor signal is wirelessly transferred to a personal computer through a wireless-fidelity DAQ card for wavelet analysis. DWT, non-decimated wavelet transform (NDWT), and dyadic wavelet transforms techniques are used for the analysis of digitized magnetic

Table 1. Literature survey on recent research in IM rotor fault detection.

Reference/year	Sensor/model parameter	Method/algorithms	Advantages and disadvantages
[34]/2020	Current sensor (current clamp)	Short-time Fourier transform (STFT), Otsu's algorithm	(1) Fixed-size window limitation in STFT (2) False fault indication in current signal analysis
[35]/2020	Time-stepping analytical model	A winding function-based mathematical model	(1) Focused on the mathematical model (simulation results)
[36]/2020	Wireless smart sensors (vibration and current sensors)	Discrete Fourier transform	(1) Resolution limitation in the Fourier analysis (2) Need expensive DAQ device
[37]/2020	Full-wave bridge rectifier (rectified current signal is used for analysis)	Discrete Fourier transform	Resolution limitation in the Fourier analysis
[4]/2019	UWB radar	Fast Fourier transform, discrete Fourier transform	Translation-invariance limitation in DWT
[38]/2019	Voltage, current synthetic waveforms	Demodulation technique	Focused only on inverter fed IM
[39]/2019	Coil sensor (magnetic signal analysis)	Spectral subtraction analysis	Less sensitivity of coil sensor
[40]/2019	Magnetic flux density-based mathematical model	Time-stepping finite element analysis	(a) Longer execution time to execute finite element analysis (b) Round off error due to finite element analysis
[41]/2019	Flux sensor (stray flux analysis)	Finite element analysis, fast Fourier transform	(1) Longer execution time (2) Resolution limitation
[42]/2019	Helmholtz flux coil (stray flux analysis)	Spectrum analysis (FFT)	(1) Less sensitivity of flux coil (2) Resolution limitation
[43]/2019	Dual search coil (rotational magnetic field analysis)	FEM	(1) Longer execution time due to the FEM analysis (2) Round off error due to the finite element analysis
Proposed work	GMR sensor identifies the rotor fault through outward magnetic flux due to broken rotor 	The GBR method is proposed which consists of hybrid NDWT analysis and LS-SVM method for rotor faults detection at earlier stage using outward magnetic radiation signal	(a) Good sensitivity (b) Translation-invariance limitation resolved through hybrid wavelet analysis (c) Real environment IM condition monitoring implemented through IoT

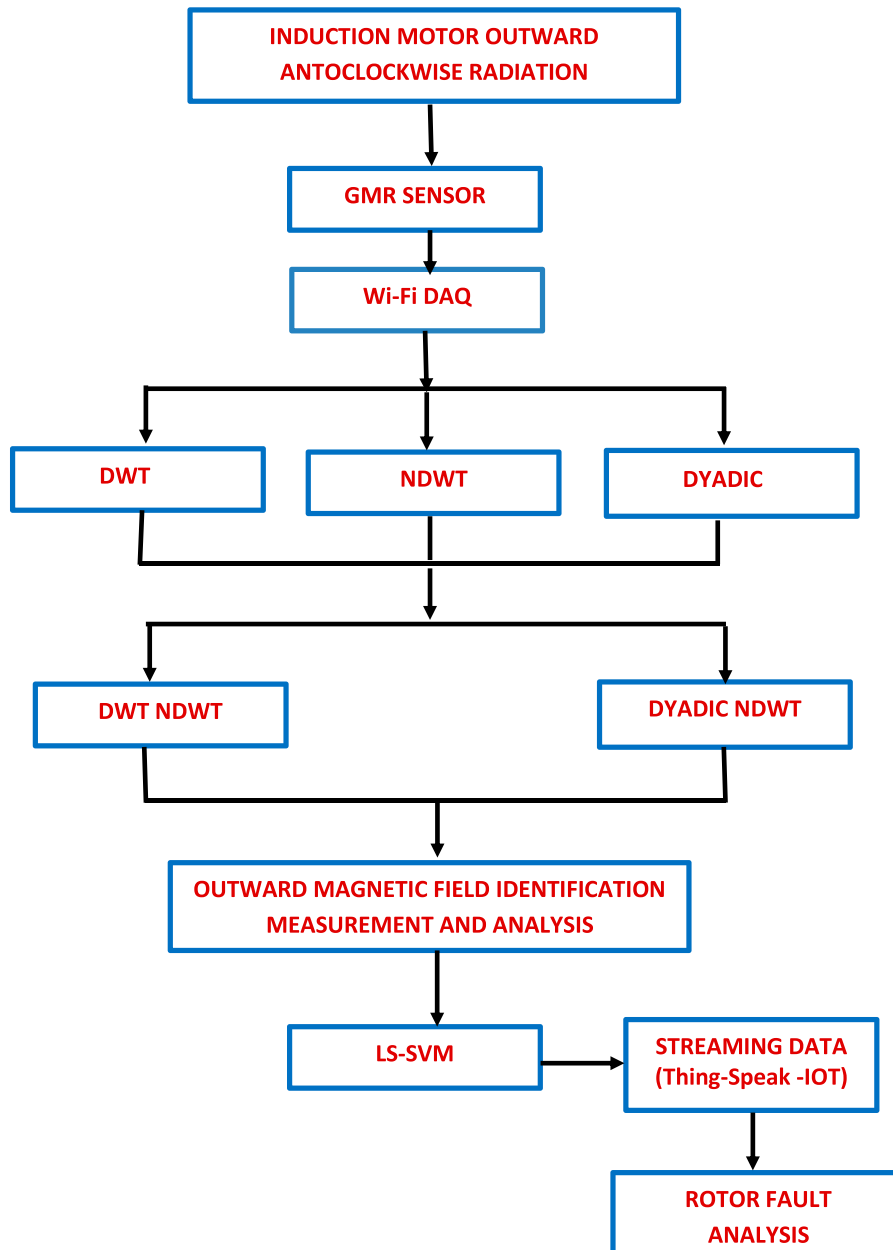


Figure 1. Methodology of the proposed GBR framework for rotor fault detection.

signatures of IM for rotor fault detection. The hybrid wavelet analysis is executed to obtain the sensitivity and specificity for rotor fault detection. In the GBR method, rotor faults are diagnosed through the hybrid wavelet analysis and least square-support vector machine (LS-SVM). The condition of IM in run-time is remotely monitored continuously through ThingSpeak IoT. Rotor bar fault condition is examined by the remote observer by the outward anti-clockwise radiation behaviour of IM based on load conditions signal data from ThingSpeak – IOT.

3.1. Anti-clockwise outward magnetic field measurement from broken rotor

The proposed GBR method identifies broken rotor bar faults by the analysis of the outward magnetic field. The balanced three-phase IM always generates a clockwise

rotating magnetic field under healthy operating conditions. There is no anti-clockwise field for a healthy electric motor [44]. An anti-clockwise magnetic field generated by the motor during rotor faults is due to the imbalance of rotor bar currents. Hence, analysis of the anti-clockwise outward magnetic field can identify the rotor bar faults detection. The anti-clockwise outward magnetic is due to motor axial and transverse components. Hence, the outward anti-clockwise magnetic field is measured based on axial-radial decomposition characteristics [45]. According to the axial-radial position of the motor, the sensor is placed at the outer stator position along the rotor axis and monitors the outward magnetic field with minimum effect of the transverse field.

In this paper, anti-clockwise outward magnetic field analyses are performed with minimal components for hardware such as GMR sensor and Wifi-DAQ. The

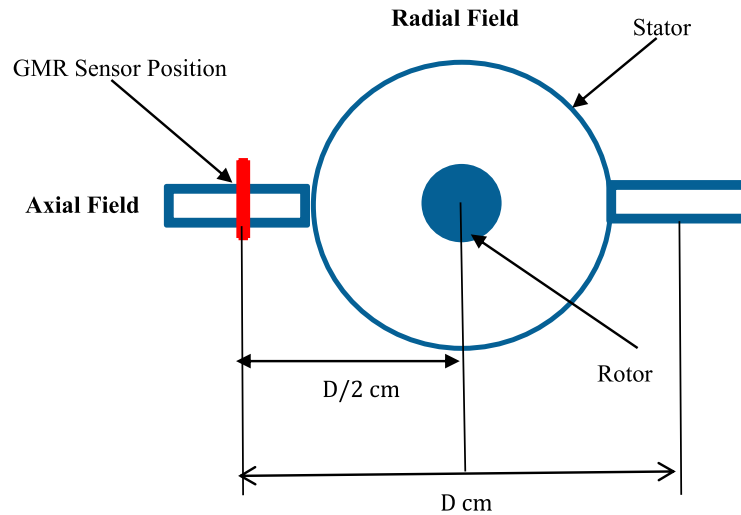


Figure 2. Optimized location of the GMR sensor for outward magnetic field acquisition and measurement.

emitted outward magnetism of IM is absorbed by the GMR sensor. The GMR sensor has high signal sensitivity and high-temperature stability. It is small in dimension compared with existing sensors such as search coil, piezo electric, acceleration, and Hall effect sensor. Therefore, the GMR sensor should be placed in an optimized location for attaining good sensitivity. The optimized placement of the GMR sensor in IM is shown in Figure 2. The sensor is focussed on the stator outer region in $D/2$ cm distance and acquires an outward magnetic field with good sensitivity and minimum transverse field radiation. The magnetic spectrum is acquired by the GMR sensor and wirelessly transmitted to the personal computer through a Wi-Fi DAQ card. The GMR sensor signal received through the Wi-Fi DAQ card is recorded by the data acquisition software (SIGVIEW) and saved as a Microsoft Sound file (*.wav). This dot wav format of the outward magnetic signal of IM is analysed by non-hybrid and hybrid wavelet transforms, and the rotor condition is monitored through anti-clockwise magnetic flux outward spectrum signals from wavelet transform coefficients.

3.2. Outward anti-clockwise magnetic field spectra analysis (non-hybrid transform)

Fast Fourier transform (FFT) is mainly used for frequency-based signal analysis for IM rotor fault detection [46]. FFT-based power spectral analysis of the IM error signal computes the peak value of the asymmetric rotor harmonics [4]. However, rotor bar failure harmonics are undifferentiated in FFT analysis, according to the research findings and experimental results [47]. The Fourier analysis method leads to inaccurate rotor fault diagnosis due to drifts and abrupt changes. To overcome the above limitations of Fourier-based motor signal analysis, short-time Fourier transform (STFT) is used as an alternative method for motor

signal analysis. STFT performs time and frequency analysis simultaneously in a signal. It has a fixed-size window during the analysis of a signal, whereas signal analysis for broken rotor needs reliable and varying window for accurate rotor fault diagnosis. Wavelet analysis is preferred for rotor fault detection in IM [48]. Wavelet transform has [49] variable window size and time–frequency domain analysis. Wavelet transform analysis provides time and frequency information of a signal by expressing the signal as a series of oscillatory functions. In wavelet transform, an input signal is decomposed and information is localized in time-scale plane, which is appropriate for the non-stationary signal analysis for IM rotor fault detection. In this paper, a unique hybrid wavelet analysis for outward anti-clockwise magnetic spectra is implemented by the hybridization of DWT, NDWT, and dyadic wavelet transform.

3.2.1. DWT decomposition of signals from constant speed of the motor with broken rotor condition

The outward anti-clockwise magnetic signal of the GMR sensor is analysed by DWT and detect broken rotor fault from signals at different harmonics. In this paper, DWT is selected because of its localized signal analysis ability. Due to this ability, DWT analysis differentiates the rotor fault signal from the sensor, even at low, medium and high speed conditions of IM. Moreover, DWT provides a better time resolution in lower and higher frequencies. Hence, DWT is suitable for the detection of rotor faults in outward anti-clockwise magnetic spectra. DWT analysis of GMR signal at multiple bands frequencies and resolutions are obtained after decomposing into a set of wavelet approximates and detailed information. DWT decomposition of outward anti-clockwise magnetic field spectrum is shown in Figure 3. The decomposition of outward anti-clockwise magnetic signals identifies frequency sub-bands through low-pass filter banks such

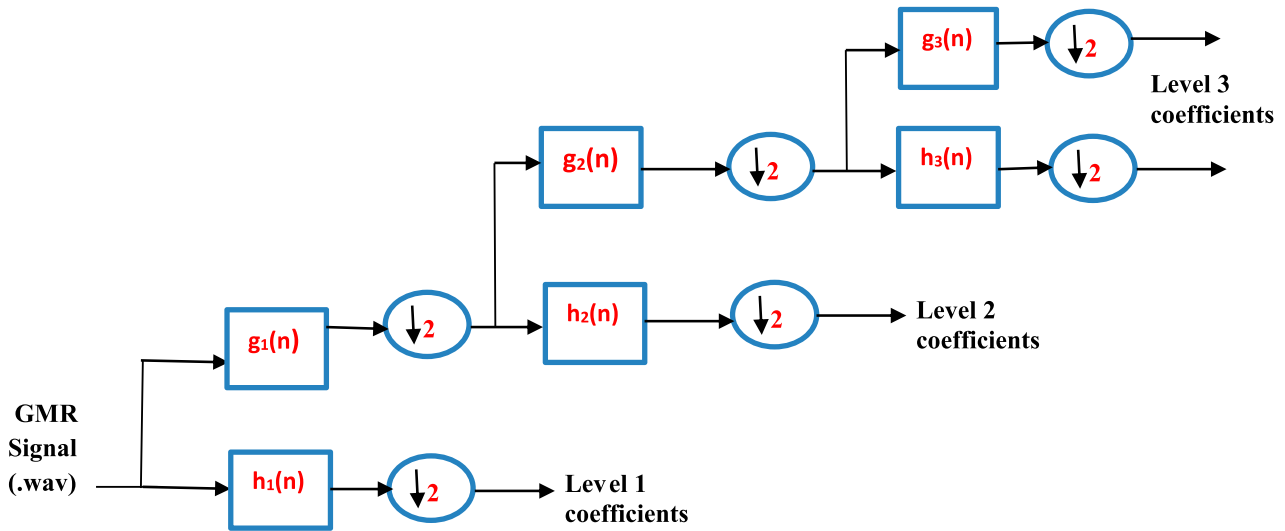


Figure 3. DWT decomposition of the outward magnetic field signal coefficients acquired through the GMR sensor.

as $g_1(n)$, $g_2(n)$, $g_3(n)$ and high-pass filter banks $h_1(n)$, $h_2(n)$, $h_3(n)$. High-frequency detailed component D_j and low-frequency approximation A_j are the down-sampled outcomes of the three-level DWT decomposition process, represented by Equations (1) and (2). The decomposed magnetic spectrum is analysed in the time–frequency domain and detect rotor fault from outward anti-clockwise magnetic signal.

$$D_j^k = \sum_n h_{n-2k} A_{j-1}^k \quad (1)$$

$$A_j^k = \sum_n g_{n-2k} A_{j-1}^k \quad (2)$$

3.2.2. NDWT decomposition to overcome translation invariance

DWT has localized signal analysis ability, superior time resolution in lower and higher frequencies. However, due to lack of translation-invariance, DWT produces a similar output during the variable speed of the motor with broken rotor condition, irrespective of the rapid shifting in GMR response signal. Due to this limitation, DWT alone is inadequate to monitor the IM conditions continuously for an extended period. In this

paper, NDWT is used to overcome the translation-invariance limitation of DWT. The lack of translation-invariance is restored in NDWT by eliminating down samplers. The NDWT is implemented by dilating original wavelet kernels (ψ , ϕ) through interpolating 2^{j-1} zeros between original wavelet kernel terms. The k th decomposition of kernels (ψ , ϕ) is specified in Equations (3) and (4).

$$\psi_j[2^{j-1}k] = \psi[k] \quad (3)$$

$$\phi_j[2^{j-1}k] = \phi[k] \quad (4)$$

NDWT decomposition process is shown in Figure 4. The decomposition of GMR outward anti-clockwise magnetic signal into frequency sub-bands is performed by low-pass filter banks such as $g_1(n)$, $g_2(n)$, $g_3(n)$ and high-pass filter banks such as $h_1(n)$, $h_2(n)$, $h_3(n)$. In NDWT, decomposed outward magnetic field signal is never downsampled, as in DWT decomposition.

3.2.3. Dyadic wavelet decomposition for medium-speed running broken rotor motor

Dyadic wavelet transform is scalable with half of the input bandwidth. Due to scaling ability, dyadic Wavelet

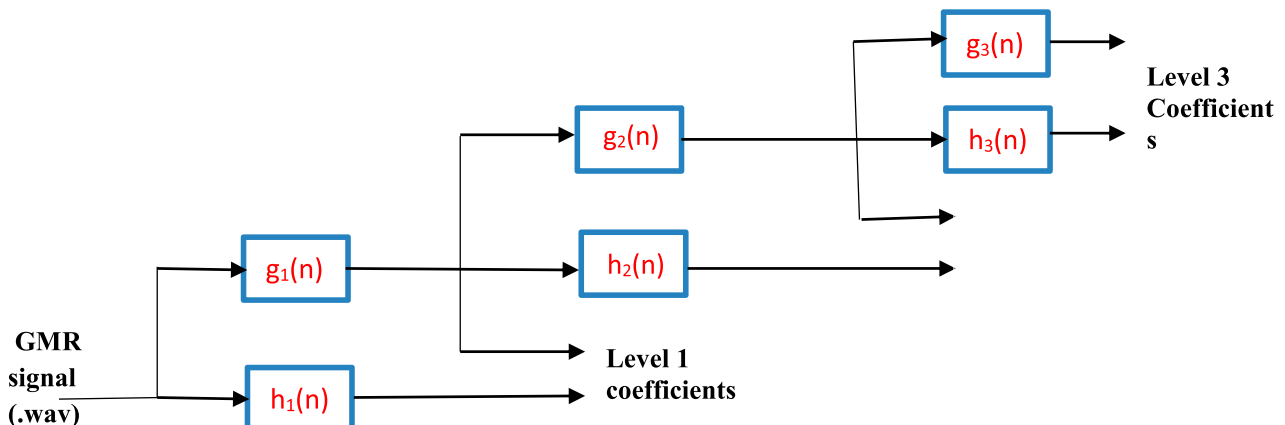


Figure 4. NDWT decomposition of the outward magnetic field signal without the downsampler.

is suitable for analysing multiple harmonics of the outward anti-clockwise magnetic signal spectrum with minimum computational complexity. Dyadic transformation is computed by dilating the selected mother wavelet with the power of two. In this paper, the quasi-spline mother wavelet function is used. The dyadic dilation at level j is as in the following equation:

$$\psi_{2^j}(x) = \left[\frac{1}{2^j} \right] \psi \left[\frac{x}{2^j} \right] \quad (5)$$

where ψ is the quasi-spline mother wavelet with zero mean value. The wavelet transform of a signal $f(x)$ at the dyadic scale 2^j and the location x are specified by the following equation:

$$W_{2^j}f(x) = f * \psi_{2^j}(x) = \int f(t) \cdot \psi_{2^j}(x - t) dt \quad (6)$$

The dyadic wavelet transform ($W_{2^j}f(x)$) is formed by the convolution of the quasi-spline mother wavelet $\psi_{2^j}(x)$ and its dyadic dilated function. The derived resultant dyadic wavelet transform operator is as the following equation:

$$D(f) = (W_{2^j}f(x))_{j \in \mathbb{Z}} \quad (7)$$

$D(f)$ denotes the dyadic wavelet transform operator. For each dyadic scale 2^j , the dyadic transform decomposes the GMR-acquired outward anti-clockwise magnetic signal into detailed coefficient ($W_{2^j}^d f$) and approximation coefficient ($s_{2^j}^d f$). The low- and high-frequency components of signal are expanded by the detailed, and approximation coefficients. The respective peaks are computed from the outcome of the dyadic decomposition signal.

3.2.4. Hybrid wavelet for outward anti-clockwise magnetic flux

The hybridization of wavelets is performed for localized signal analysis and translation invariance. Additional scaling in hybrid transform analysis leads to

early detection of rotor fault from outward magnetic spectrum signal. The localized signal analysis ability is attained through the Daubechies wavelet. The filter coefficient (h) of Daubechies wavelet is given in Equation (8). GMR-acquired outward anti-clockwise magnetic signal decomposition using the filter coefficient (h) retains the time and frequency domain properties of the magnetic signal and obtains the localized signal for analysis. Contrasting with DWT, NDWT is implemented with a higher rank of filters at each level for GMR-acquired outward anti-clockwise magnetic signal through decomposition. Using a higher ranking of filters at each decomposition level analyses the shift in GMR outward anti-clockwise magnetic signal. The filtering ranking is dependent and associated with the GMR signal transition and satisfies the translation-invariance property as in the following equation:

$$h = \left[\frac{(1 + \sqrt{3})}{4\sqrt{2}} \frac{(3 + \sqrt{3})}{4\sqrt{2}} \frac{(3 - \sqrt{3})}{4\sqrt{2}} \frac{(1 - \sqrt{3})}{4\sqrt{2}} \right] \quad (8)$$

In the hybridization of the wavelet transform, dyadic wavelet is considered for its additional scaling property. The additional scaling property of dyadic wavelet is represented by Equations (9) and (10).

$$\phi_1(t) = 2^{1/2} \sum_{k=0}^{M-1} g_k \phi_1(2t - k) \quad (9)$$

where $\phi_1(t)$ is the scaling function in terms of M scaling functions of $\phi_1(2t - k)$ with a double resolution. Here g is the coefficient of amplitude for $k = 0, 1, \dots, M - 1$. The scaling function on the right-hand side of the equation (9) is agreeable to the dilated second expansion. Hence Equation (9) becomes as Equation(10).

$$\phi(2t - k) = 2^{1/2} \sum_{k=0}^{M-1} g_j \phi_1(2[2t - k] - j) \quad (10)$$

when Equation (10) is substituted to the right-hand side of Equation (9), the outcome is an expression of

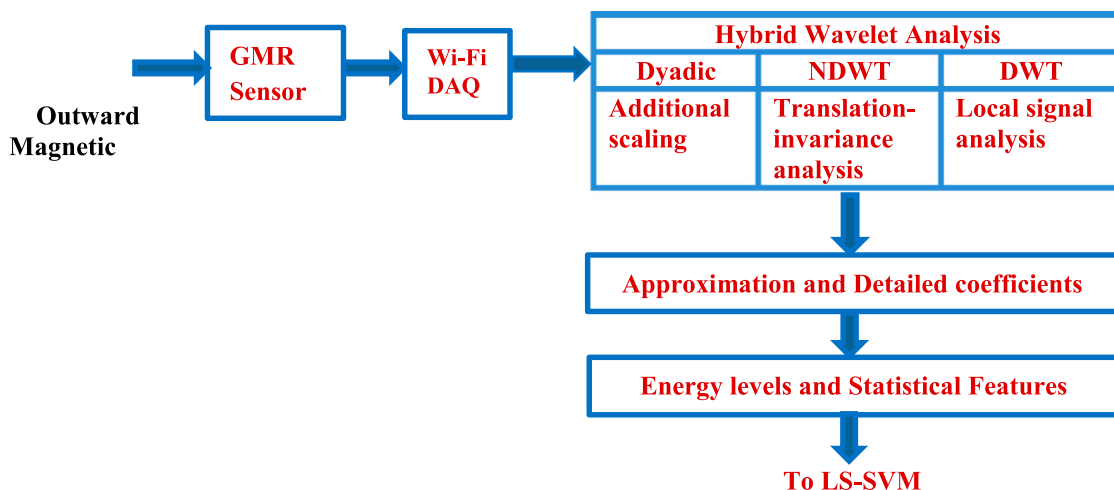


Figure 5. Hybrid wavelet analysis of the outward magnetic spectrum signal acquired from the GMR sensor.

$\varphi(t)$, which contains M^2 scaling functions. These additional scaling functions build the dyadic Wavelet as an optimized wavelet and analyse the different harmonics in outward magnetic spectra with minimum computational complexity. The sequential implementation steps of the hybrid wavelet analysis are illustrated in Figure 5. The GMR-acquired outward anti-clockwise magnetic signal is sequentially decomposed by the dyadic Wavelet for extra scaling, NDWT for translation-invariance, and DWT for localized signal analysis. The approximation and detailed coefficients are derived as the outcome of the hybrid wavelet decomposition. The multiresolution outcomes of different frequency bands of decomposed GMR-acquired outward anti-clockwise magnetic signal are used as input for feature extraction for broken rotor fault diagnosis and detection. The energy levels and statistical features such as mean (μ), standard deviation (σ), skewness (S), kurtosis (K) are extracted from the decomposed frequency bands. The energy level computation of each sub-band is performed through the following equation:

$$E_j = \sum_{k=1}^{k=n} |D_{jk}(n)|^2 \quad (11)$$

where j is the hybrid wavelet decomposition level. The energy level of decomposed GMR-acquired outward anti-clockwise magnetic signal is related to the severity of the fault and identifies the broken rotor fault at an early stage. The mean value of the wavelet sub-band indicates the variations due to the rotor fault in IM. The other statistical features such as standard deviation, kurtosis and skewness are the amplitude shape descriptors and differentiate the variation between the healthy rotor and broken rotor of IM.

3.2.5. Fault detection and monitoring through LS-SVM classification

The least square-supported vector machine algorithm classifies the IM conditions such as healthy or broken rotor fault from wavelet sub-band energy levels and statistical features. The classical SVM is used in several real-time classification problems. However, additional computational steps are required for the quadratic solution, which is the major constraint of classical SVM. In LS-SVM, the quadratic solution limitation of the SVM is modified by linear equations, which require minimal computational steps [50]. LS-SVM achieves good classification accuracy even for a small training database. In this paper, LS-SVM is used for IM rotor fault diagnosis. LS-SVM is trained by the training dataset, which contains the energy levels and statistical features of the IM outward magnetic signal from healthy and faulty rotors. These features are extracted through hybrid wavelet analysis such as DWT-NDWT and Dyadic-NDWT of magnetic signals acquired from

the healthy and faulty broken rotor of IMs. LS-SVM finds optimal hyper-plane (OHP) with the highest margin and separates the wavelet feature data points into two categories as healthy or faulty. The representation of OHP in feature space is as in the following equation:

$$y(f) = \omega^T \Phi(f) + b \quad (12)$$

$y(f)$ is the classification outcome for healthy or faulty IM, which is obtained from the input wavelet feature set f , ω is the normal vector of the OHP. The maximum margin of the OHP is achieved by minimizing the squared average value of the normal vector (ω). The broken rotor fault decision functions of the LS-SVM depend on kernel functions. Hence, selecting an optimum kernel function for the LS-SVM classifier is essential for accurate IM fault diagnosis. Normally, local and global kernels are used in the LS-SVM, for decision making [51]. In this paper, the radial basis function (RBF) kernel is used as the local kernel. The RBF kernel is selected because of translation-invariance property and differentiates the broken bar outward anti-clockwise signal from a healthy motor signal. Due to translation-invariance property, RBF kernel can build an accurate decision function for translation-invariant of wavelet features. The RBF kernel is given as in the following equation:

$$K_{\text{RBF}} = \exp(-x - x_i^2/\sigma^2) \quad (13)$$

σ is the RBF kernel's width polynomial kernel, a global kernel is selected for broken rotor classification. The polynomial kernel is as in the following equation:

$$K = (1 + x_i^T x)^d \quad (14)$$

" d " is denoted as the kernel parameter. Utilizing the RBF, polynomial kernel functions in LS-SVM lead to binary classification of healthy or broken rotor fault from IM magnetic signal. Furthermore, the condition of the IM is remotely monitored by the observer through cloud ThingSpeak IoT. For continuous monitoring of IM, a channel-based online application is created using ThingSpeak. The cloud ThingSpeak is linked to the MATLAB software for constant monitoring of outward magnetic spectrum's wavelet parameters during the run-time of IM. For any abnormal IM operation condition, an instant warning message will be generated through the ThingSpeak IOT application.

4. Results and discussions

4.1. Experimental set-up

The parameters of the IM used in our experiment are presented in Table 2. The proposed GBR method has been implemented and evaluated for the healthy and faulty operating conditions of IM. In this experiment, initially healthy motor outward magnetic signals are collected following from the broken rotor of IM. The



Figure 6. The hardware set-up of the proposed framework for IM rotor fault diagnosis.

rotor fault was artificially created by drilling holes on the rotor bar of IM, which is known as the super drilling technique. The hardware set-up of the proposed framework for IM rotor fault diagnosis is shown in Figure 6. Furthermore, the GMR sensor acquires outward magnetic signal from IM at different locations along the rotor axis, such as 10, 20 cm between the rotor axis and the GMR sensor. The magnetic spectrum acquired by the GMR sensor is transferred through Wi-Fi DAQ to the personal computer (PC) with a configuration of 2.40 GHz frequency Intel Core i3 processor and 4GB RAM. In PC, the magnetic spectrum is acquired by MATLAB acquisition toolbox at the sampling rate of 22,050 Hz and acquired signals are saved as Microsoft dot wav files. These GMR-acquired signals are inferred with hybrid wavelet analysis such as DWT-NDWT and Dyadic-NDWT and extract the rotor fault features through coefficient energy level and LS-SVM classifier for IM rotor fault diagnosis. The optimized hybrid wavelet analysis and LS-SVM-based fault detection are implemented using the MATLAB 2018a software. The condition monitoring of rotor magnetic signal parameters is implemented using the ThingSpeak cloud.

4.2. Optimization of GMR sensor location for acquiring outward magnetic signal from IM

The outward anti-clockwise magnetic spectra are acquired by the GMR sensor at 10 and 20 cm distance from the rotor axis of an IM and shown in Figures 7 and 8. Figure 7 shows the broken rotor IM signal and has

Table 2. Parameters of the IM used in the experiment for rotor fault detection.

Power	1 HP (0.75 kW)
Current	2.5 A
Synchronous speed	1500 rpm
Speed	1440 rpm
Power supply details	415 V, 3-phase, 50 Hz
WIFI-DAQ	Lab Jack-Model No T7-Pro
GMR sensor	NV Electronics-AA002 Sensor

a normalized RMS value of about 0.3350 mv, which is less than the healthy IM normalized RMS value 0.3530 mv, when the outward magnetic signal is acquired from a 10 cm distance. The normalized RMS of the outward magnetic spectrum is less for a broken rotor of IM due to the imbalanced magnetic field produced by the broken rotor bar current. The broken rotor bar in IM, current causes unbalanced oscillations in outward anti-clockwise magnetic signal, which is highlighted in Figures 7(b) and 8(b). Figures 7(a) and 8(a) show the harmonics of the outward anti-clockwise magnetic signal of the healthy IM and magnetic field distributed evenly without any unbalanced oscillations. The reason for the even distribution of the magnetic spectrum is the absence of an anti-clockwise field. Figure 8 shows the acquired outward magnetic flux signal at 20 cm distance, and the broken rotor IM normalized RMS value of the amplitude is 0.225897 mv, which is significantly less than the healthy IM normalized RMS value of 0.4600 mv. The difference in normalized RMS value of healthy and broken rotor IM magnetic spectrum is significantly observable at 20 cm distance, compared with 10 cm distance. Moreover, Figures 7 and 8 show normalized RMS of the magnetic signal acquired at 10 cm distance, which is less than the normalized RMS of the magnetic signal acquired at 20 cm distance due to axial-radial decomposition characteristic. When the GMR sensor is placed closer to IM during the acquisition of emitted magnetic spectrum, the normalized RMS of amplitude is reduced due to the transverse magnetic field, caused by the IM. Hence, 10 cm distance is avoided and 20 cm distance along the rotor axis is considered the optimum location for outward magnetic spectrum acquisition.

4.3. Hybrid wavelet analysis and fault signature extraction for low- to high-speed motor running with broken rotor

Hybrid wavelet analysis for the outward anti-clockwise magnetic signal is acquired at 20 cm distance and DWT,

NDWT, and dyadic wavelet NDWT transform are applied. The level of decomposition for hybrid wavelet analysis is computed using the following equation:

$$n > \text{int} \left(\frac{\log \left(\frac{f_e}{f_s} \right)}{\log(2)} \right) + 1 \quad (15)$$

“ n ” is the number of hybrid wavelet decomposition levels, f_e (22.050 kHz) is the sampling frequency of the acquired IM magnetic signal [52], f_s (50 Hz) is the fundamental frequency of the IM magnetic spectrum. The frequency component of the outward anti-clockwise magnetic field signal ranges between 0 and 22,050 Hz. In this experiment, 22,050 Hz outward magnetic spectra of healthy and broken rotor IM signals are decomposed into ten frequency sub-bands through the hybrid wavelet analysis. Among the hybrid wavelet analyses, such as Dyadic-NDWT and DWT-NDWT, The Dyadic-NDWT analysis shows better results and is verified through RMS values. Table 3 provides the association between the ten levels of Dyadic-NDWT wavelet coefficients and their range of frequencies of Dyadic-NDWT. In Table 3, 24.96 Hz frequency is

associated with L10 decomposition. The IM with rotor bar fault vibrates at 40–48 Hz characteristic frequency range at the level of 9th decomposition (L9) and higher-order harmonics range 240–260 Hz frequencies at the level of 7th decomposition (L7).

In the Dyadic-NDWT hybrid wavelet signal analysis, wavelet sub-bands are computed after the repeated acquisition of outward magnetic spectra of IM with healthy and broken rotor conditions with low, high and medium-speed running of the motor. The rotor vibration frequency, rotor fault frequency, and higher-order harmonics exist in L7 to L10 sub-bands of anti-clockwise outward signal magnetic signal. The wavelet sub-bands L7 to L10 of the healthy and broken rotors of IM are shown in Figures 9–12. In Figures 9–12, time (ms) is denoted in the x -axis, and amplitude (mV) is denoted in the y -axis. The healthy IM radiates a strong outward anti-clockwise magnetic signal with higher amplitude values such as (5 mV maximum peak) due to the non-existence of the anti-clockwise magnetic field, as shown in Figures 9(a) and 12(a). The broken rotor IM shows less outward magnetic field radiation amplitude due to anti-clockwise magnetic field, and shown

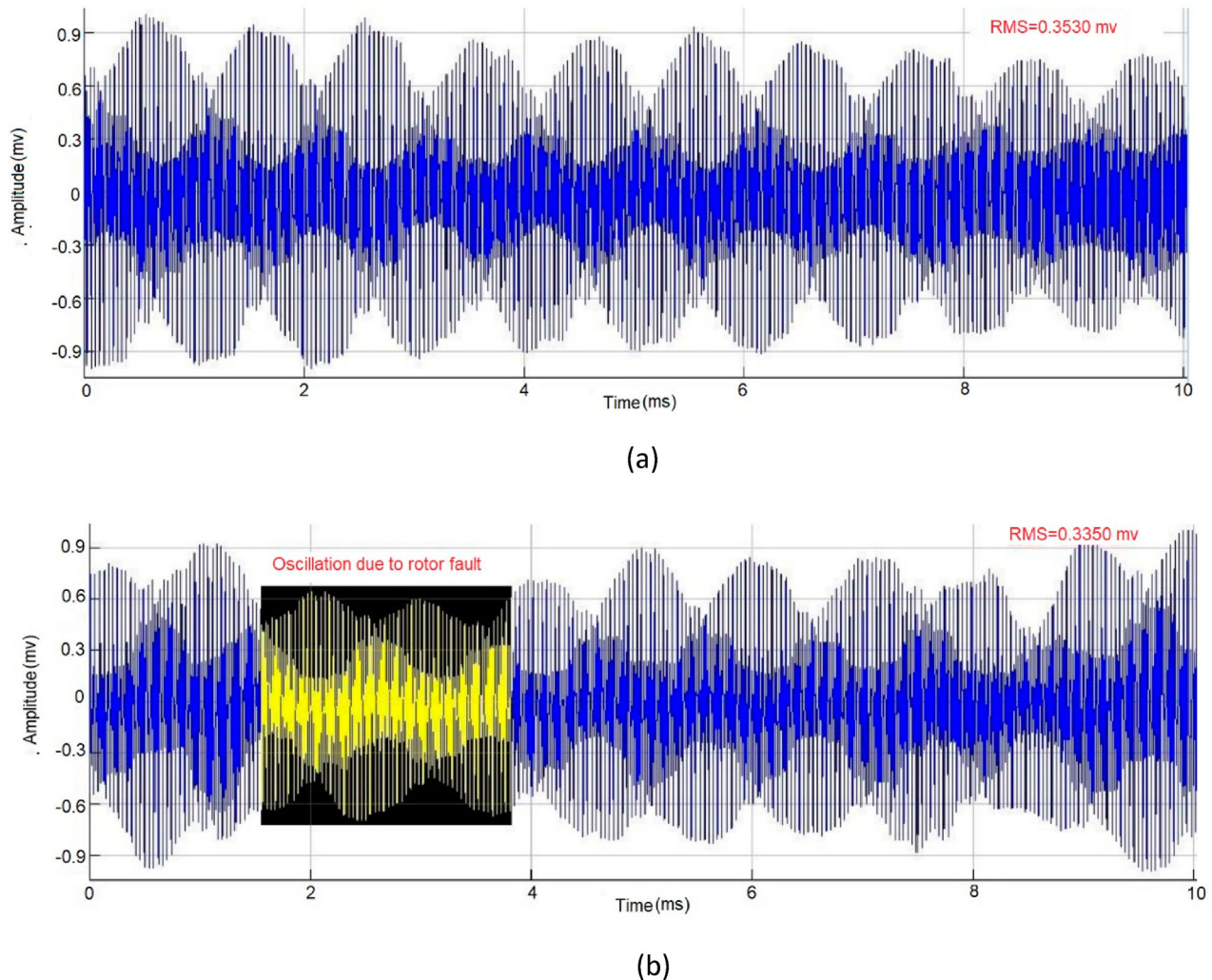


Figure 7. Outward magnetic spectrum of the IM acquired by the GMR sensor at 10 cm distance from the rotor axis: (a) IM with a healthy rotor, (b) IM with a faulty rotor.

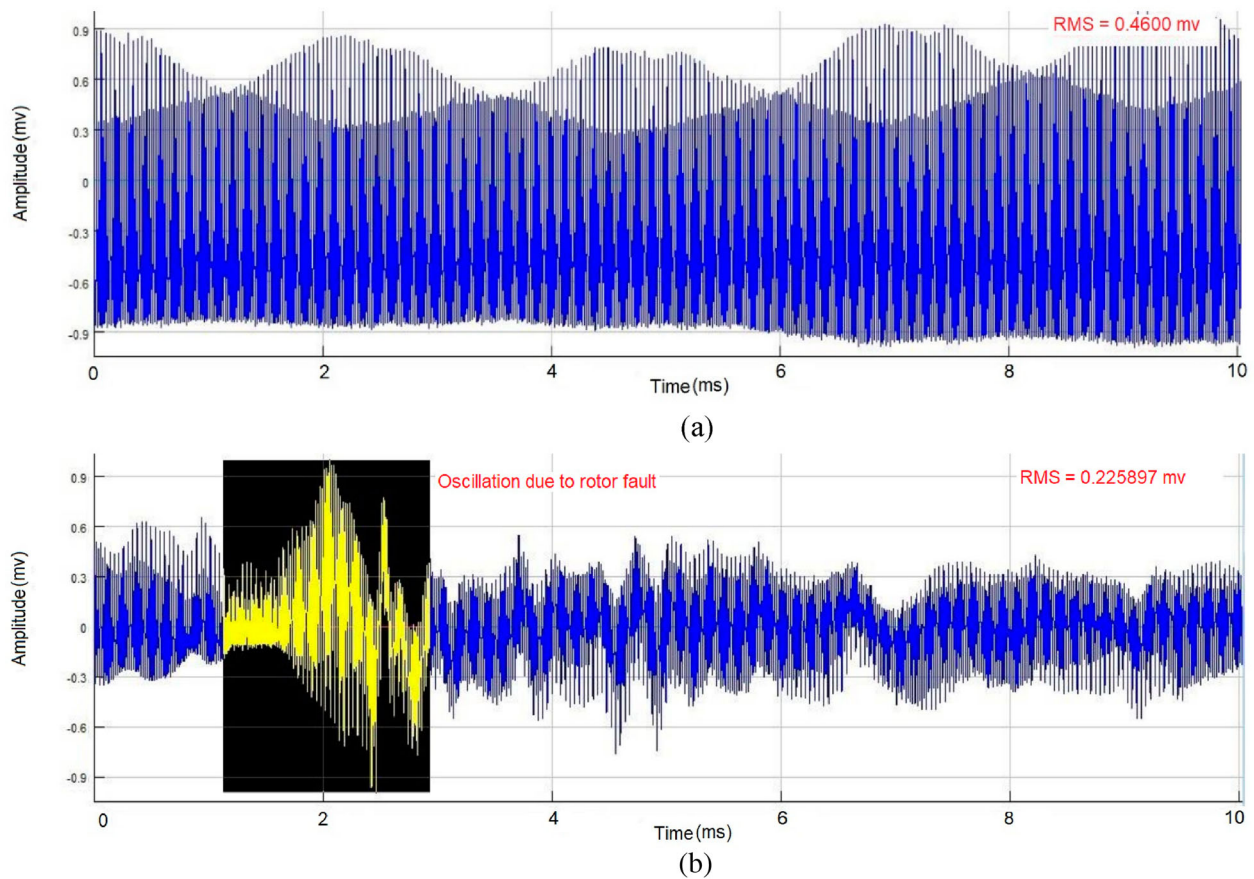


Figure 8. Outward magnetic spectrum of the IM acquired by the GMR sensor at 20 cm distance from the rotor axis: with (a) healthy rotor, (b) IM with a faulty.

in Figures 9(b) and 12(b). Figures 9(b) and 12(b) have lesser amplitude values such as (2 mV maximum peak) compared with the amplitude of healthy IM and shown in Figures 9(a) and 12(a). The maximum magnetic field radiation is in sub-band 10 for healthy IM, shown in Figure 12(a) and an amplitude value is about 5 mV. The amplitude variation is considerably observable in sub-bands 7 and 10 compared with sub-bands of 8 and 9, and shown in Figures 10 and 11. A high spectral resolution in the full load range of the machine is obtained in sub-bands.

The energy level distribution across the wavelet sub-bands of outward anti-clockwise magnetic signal is shown in Figure 13. As shown in Figure 13(a), healthy IM energy level significantly increases at sub-bands

Table 3. Frequency sub-bands of the hybrid wavelet (Dyadic-NDWT) analysis.

Decomposition level	Approximation frequency bands (Hz)	Details frequency bands (Hz)
L1	A1 0–11,025	D1 11,025–22,050
L2	A2 0–5512.5	D2 5512.5–11,025
L3	A3 0–2756.25	D3 2756.25–5512.5
L4	A4 0–1378.125	D4 1378.125–2756.25
L5	A5 0–689.0625	D5 689.0625–1378.125
L6	A6 0–344.5312	D6 344.5312–689.0625
L7	A7 0–172.2656	D7 172.2656–344.5312
L8	A8 0–86.1328	D8 86.1328–172.2656
L9	A9 0–43.0664	D9 43.0664–86.1328
L10	A10 0–21.5332	D10 21.5332–43.0664

such as D7 (62% of total energy) and D8 (27% of total energy). Figure 13(b) shows the energy level of the broken rotor of IM magnetic signal, the energy level of the sub-band D10 (84% of total energy) is increased highly, and the energy levels of the sub-bands such as D7 (8% of total energy) and D8 (7% of total energy) are decreased compared with the healthy state of IM magnetic signal. Hence, the broken rotor fault condition of IM is identified at an early stage from the energy level distribution of the wavelet sub-bands from D7 to D10. Along with these energy levels, statistical features are extracted for wavelet sub-bands coefficients and classify the healthy and broken rotor states of IM. The hybrid wavelet statistical features of healthy and broken rotor IMs are provided in Table 4. The statistical parameter of the healthy IM varies with the statistical parameter of the broken rotor IM. Hence, the extracted statistical features and energy levels are used in the LS-SVM classifier for IM rotor fault detection. The Steady-state operating conditions are analysed. The statistical study based on the calculation of the correlation coefficient of each signal is performed.

4.4. Broken rotor fault detection and evaluation

Statistical features and energy levels of the Dyadic-NDWT hybrid wavelet frequency sub-bands are used for fault signature identification of the broken rotor

of IM. These features are extracted from the outward anti-clockwise magnetic signals from healthy and faulty rotors of IMs running in different speed conditions. Fifty magnetic signals are acquired through DAQ and Matlab software at low, medium and high speed conditions. The extracted features are fed to the LS-SVM classifier along with the label (healthy or broken rotor)

to train the classifier for broken rotor detection in IM. After training, the performance of the trained LS-SVM classifier is assessed in MATLAB software through the testing process using the testing data. For training, 60% of data are used and 40% for testing data. The fault detection accuracy of the proposed GBR method is evaluated through the confusion matrix. The confusion

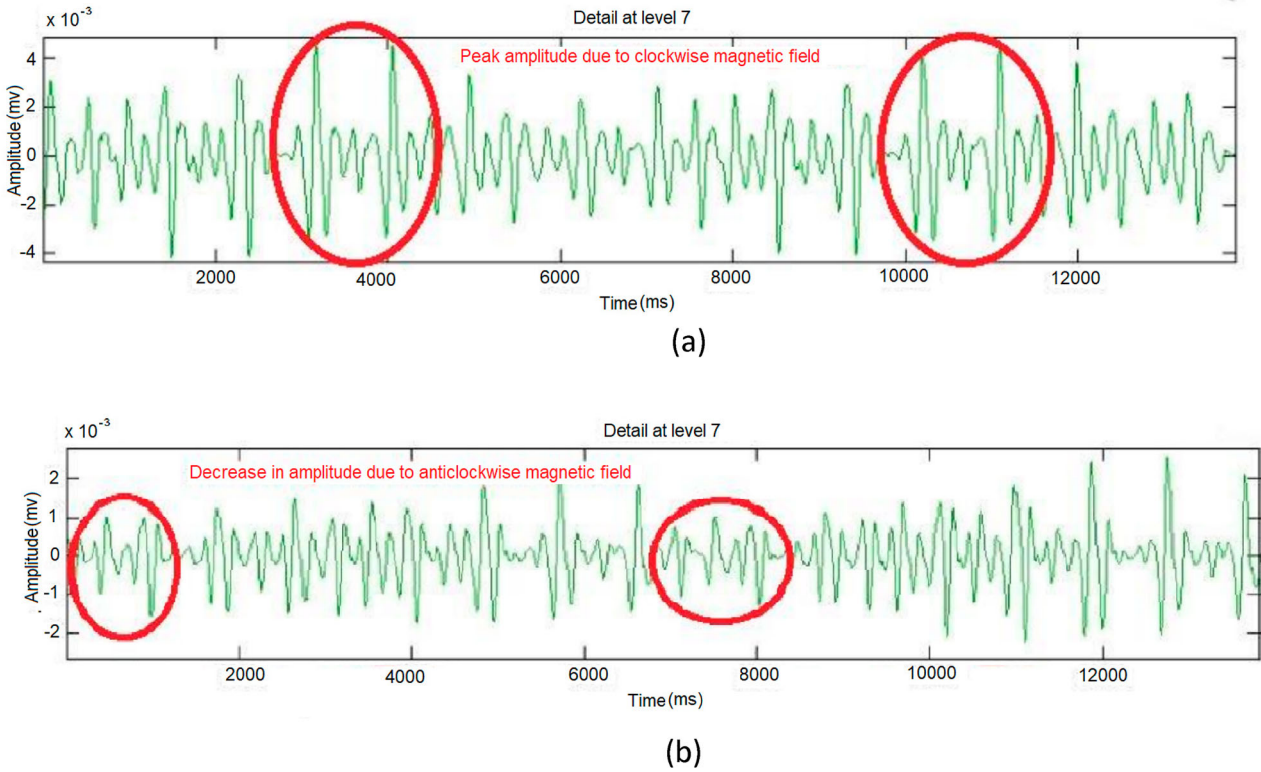


Figure 9. Wavelet sub-band 7 of the outward magnetic spectrum: (a) healthy IM, (b) IM with rotor fault.

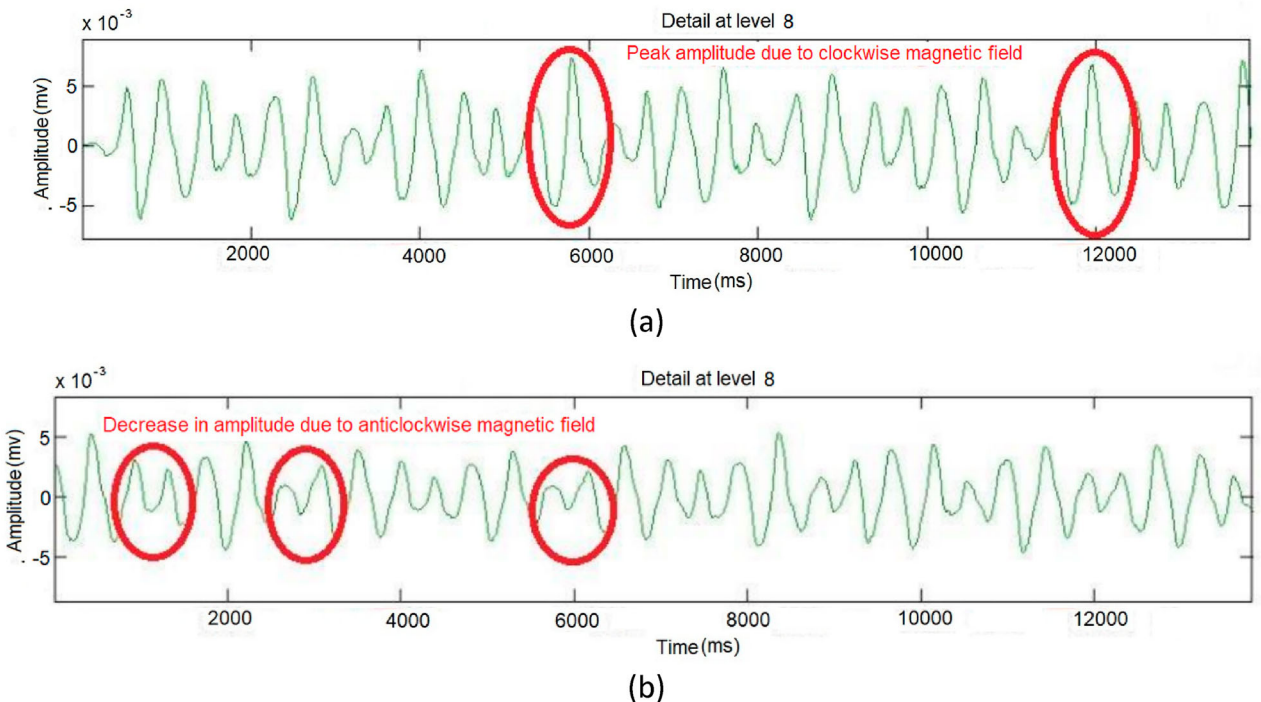


Figure 10. Wavelet sub-band 8 of the outward magnetic spectrum: (a) healthy IM, (b) IM with rotor fault.

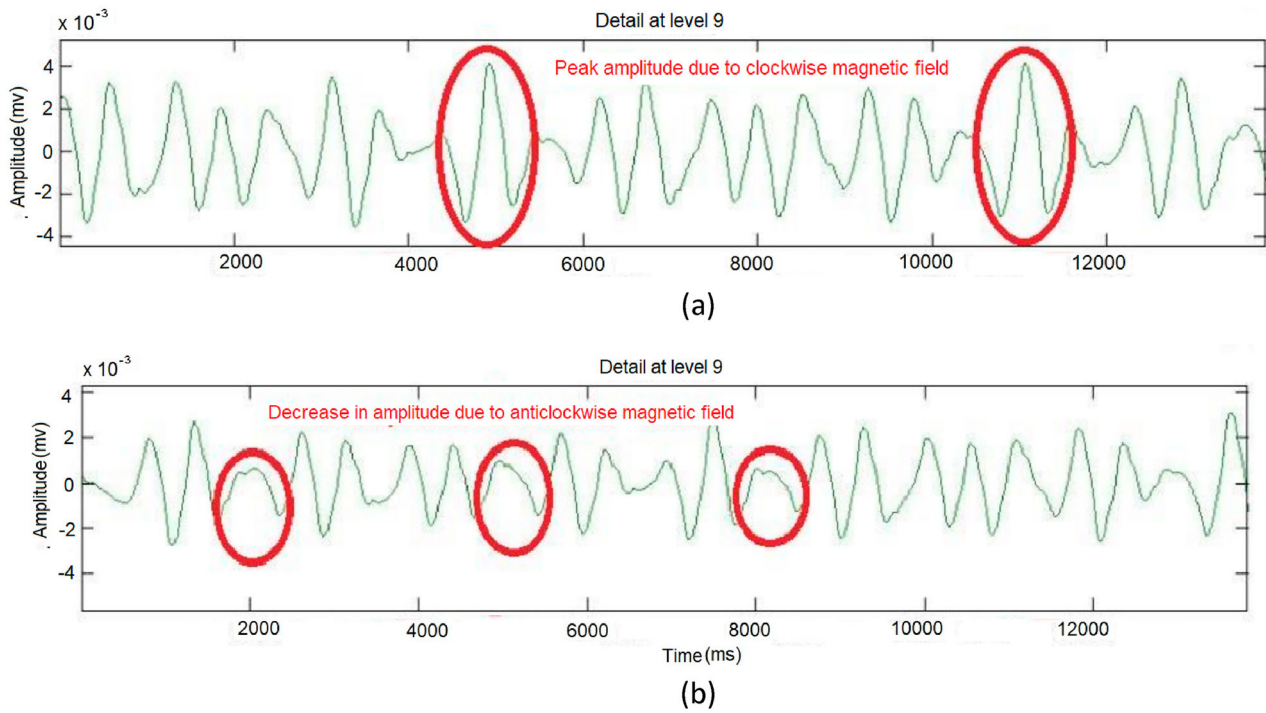


Figure 11. Wavelet sub-band 9 of the outward magnetic spectrum: (a) healthy IM, (b) IM with rotor fault.

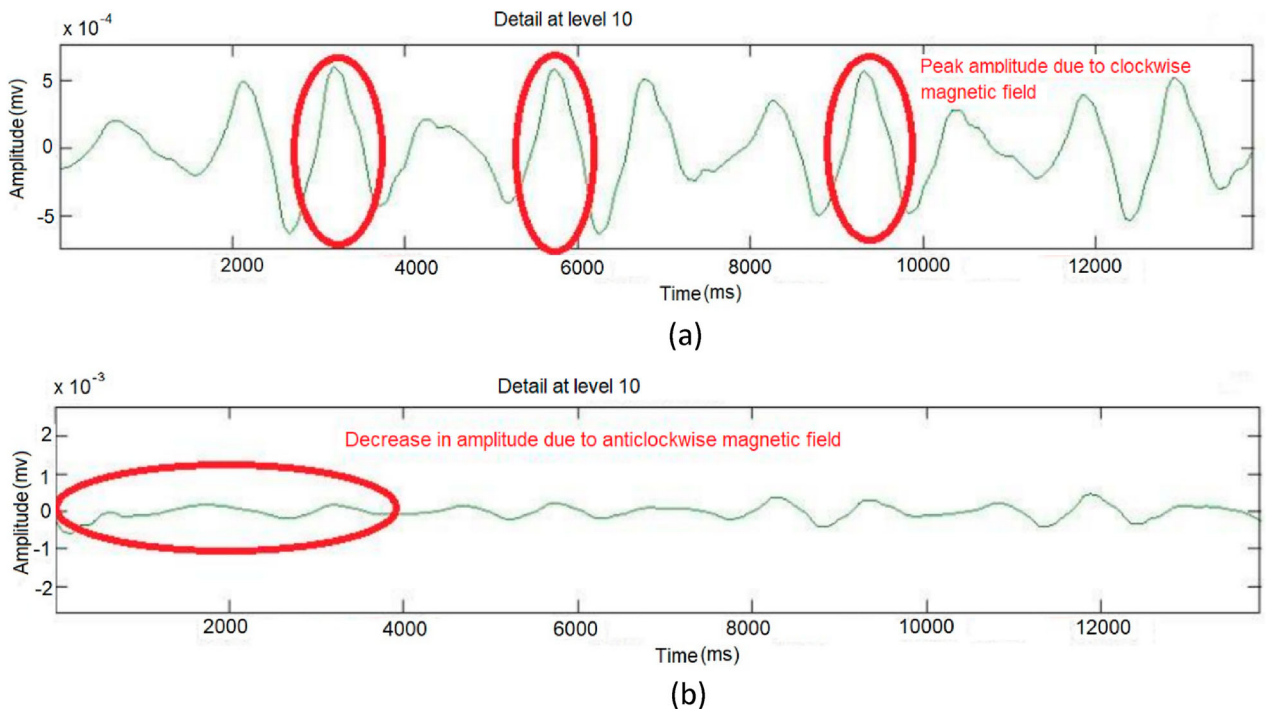


Figure 12. Wavelet sub-band 10 of the outward magnetic spectrum: (a) healthy IM, (b) IM with broken rotor fault.

matrix has recognized the classification outcome of the LS-SVM classifier in each state of fault detection, and the following four metrics are computed from the confusion matrix such as (i) True Positive (TP), (ii) False Positive (FP), (iii) True Negative (TN) and, (iv) False Negative (FN). For the broken rotor fault in IM, the outcome is TP, where the classifier outcome is faulty, and FN is the classifier outcome for the healthy rotor

of IM. For the healthy rotor in IM, the outcome is TN, where the classifier outcome is healthy, and FP for classifier outcome is faulty. Table 5 shows broken rotor metrics. The confusion matrix of the LS-SVM classifier for IM fault diagnosis using the test data is given in Table 5. The sensitivity, specificity, and classification accuracy of LS-SVM classifier in IM broken rotor fault detection in IM are computed from Table 5 using equations

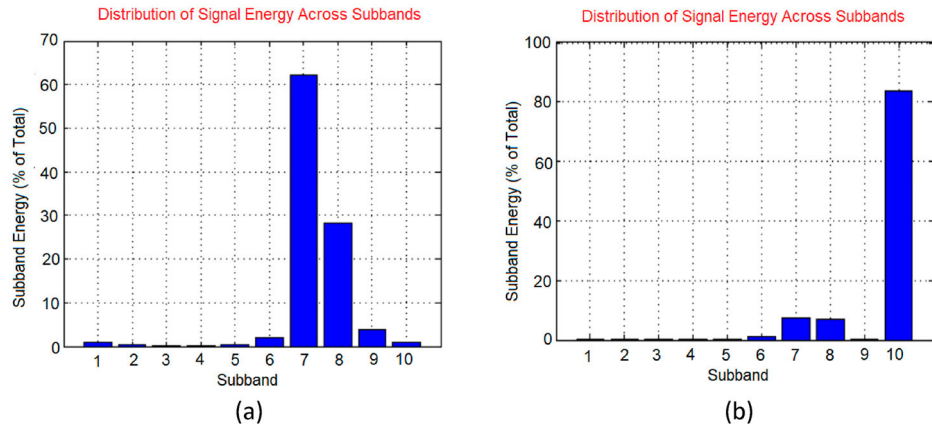


Figure 13. Distribution of magnetic signal energy across the wavelet sub-bands: (a) healthy IM, (b) faulty IM.

(16) to (18).

$$\text{Sensitivity}(\%) = \frac{\text{TP}}{\text{TP} + \text{FN}} \times 100\% \quad (16)$$

$$\text{Specificity}(\%) = \frac{\text{TN}}{\text{TN} + \text{FP}} \times 100\% \quad (17)$$

$$\text{Accuracy}(\%) = \frac{\text{TP} + \text{TN}}{\text{TP} + \text{TN} + \text{FP} + \text{FN}} \times 100\% \quad (18)$$

The proposed GBR method attained 95% sensitivity, 90% specificity, and 92.5% classification accuracy for rotor fault detection in IM. The classification outcome shows the diagnostic efficiency of the proposed GBR method in IM rotor fault detection and is significantly better than other existing methods. To monitor, the rotor's faulty condition continuously during run-time and analyse outward anti-clockwise signal behaviour, signal data are uploaded in ThingSpeak cloud, an IoT analytics tool. Figure 14 shows the live run-time condition monitoring of IM using ThingSpeak IoT. The

Table 4. Statistical features of the hybrid wavelet analysis.

Decomposition level	Statistical features	Healthy IM	Faulty IM
L7	Mean (μ)	0.0088	0.0049
	Standard deviation (σ)	0.0081	0.0073
	Skewness (S)	0.9594	1.6160
	Kurtosis (K)	2.3954	4.3283
L8	Mean (μ)	0.0073	0.0044
	Standard deviation (σ)	0.0080	0.0071
	Skewness (S)	1.1255	1.7635
	Kurtosis (K)	2.8263	4.8716
L9	Mean (μ)	0.0063	0.0040
	Standard deviation (σ)	0.0078	0.0068
	Skewness (S)	1.2953	1.9027
	Kurtosis (K)	3.2790	5.4268
L10	Mean (μ)	0.0053	0.0036
	Standard deviation (σ)	0.0076	0.0066
	Skewness (S)	1.4598	2.0345
	Kurtosis (K)	3.8015	5.9905

Table 5. Confusion matrix of LS-SVM classifier for IM fault diagnosis.

Actual classification	LS-SVM predicted classification	
	Faulty rotor	Healthy rotor
Faulty rotor	19 (True Positive)	01 (True Negative)
Healthy rotor	02 (False Positive)	18 (True Negative)

wavelet energy levels of sub-bands and statistical features are updated in the ThingSpeak cloud storage. The ThingSpeak platform is linked with the MATLAB software for automated updates of wavelet features, and live run-time condition monitoring of the IM is performed. ThingSpeak generates warning messages for rotor faulty conditions in IM.

5. Conclusion

The broken rotor fault in IM is focused and analysed for earlier fault detection. The early stage IM rotor fault detection is challenging due to the low sensitivity of sensors and translation-invariance limitation in rotor signal analysis techniques. The proposed GBR method detects the rotor fault early from the outward anti-clockwise magnetic signal after analysis with different hybrid wavelet transform. The outward anti-clockwise magnetic signal of IM is directly associated with the broken rotor faults in IM. The magnetic signals are acquired in the outward region of the IM along the rotor axis with the GMR sensor and validated for the efficiency of acquired signals from the healthy and faulty broken rotor motor. GMR sensor signals are acquired from various positions and analysed for optimum location of GMR sensor for rotor fault identification in IM. The variances in the magnetic spectrum of the healthy and broken rotor in IM are found from GMR sensor positions such as 10 and 20 cm and observed through the normalized RMS value and the unbalanced harmonics appear in the magnetic spectra. The 20 cm distance along the rotor axis is identified as the optimum position for GMR sensor placement. Furthermore, Dyadic-NDWT hybrid wavelet analysis results show a significant change in the energy levels and statistical features of the outward anti-clockwise magnetic signal sub-bands for healthy and broken rotors of IM. In the experimental evaluation, the performance of the proposed GBR method is evaluated using 40 healthy and faulty magnetic signals of IM. The confusion matrix is used as the performance indicator for

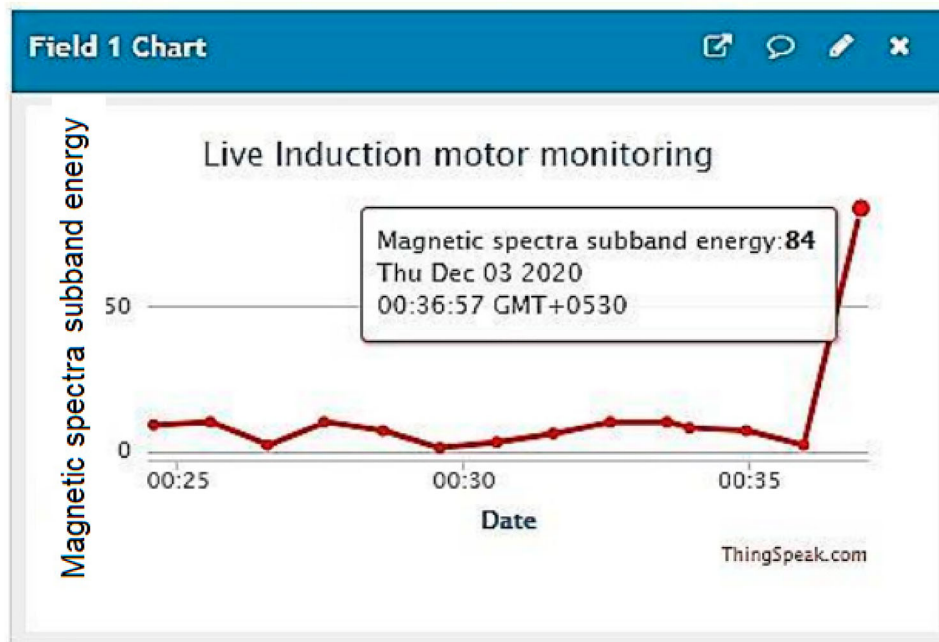


Figure 14. Run-time IM condition monitoring using ThingSpeak IoT analytics.

LS-SVM-based classification of the IM condition such as healthy or broken rotor. From evaluation results, the proposed GBR method identifies IM rotor faults with 95% of sensitivity, 90% of specificity, and 92.5% classification accuracy. The experimental results confirm that the proposed non-contact method detects the rotor faults in IM at an early stage. Moreover, ThingSpeak IoT platform-based IM condition monitoring is implemented during run-time. Magnetic anti-clockwise outward signals can be analysed with a deep learning algorithm.

Disclosure statement

No potential conflict of interest was reported by the author(s).

References

- [1] da Silva AM, Povinelli RJ, Demerdash NAO. Induction machine broken bar and stator short-circuit fault diagnostics based on three-phase stator current envelopes. *IEEE Trans Ind Electron.* 2008 Mar;55(3):1310–1318. DOI:10.1109/TIE.2007.909060
- [2] Bonnett AH, Yung C. Increased efficiency versus increased reliability. *IEEE Ind Appl Mag.* 2008 Jan;14(1):29–36. DOI:10.1109/MIA.2007.909802
- [3] Thorsen OV, Dalva M. A survey of faults on Induction motors in offshore oil industry, petrochemical industry, gas terminals, and oil refineries. *IEEE Trans Ind Appl.* 1995;31(5):1186–1196. DOI:10.1109/28.464536
- [4] Barusu MR, Sethurajan U, Deivasigamani M. Non-invasive method for rotor bar fault diagnosis in three-phase squirrel cage induction motor with advanced signal processing technique. *J Eng.* 2019;2019(17):4415–4419. DOI:10.1049/joe.2018.8242
- [5] Martinez J, Belahcen A, Arkkio A. Broken bar indicators for cage induction motors and their relationship with the number of consecutive broken bars. *IET Electr Power Appl.* 2013;7(8):633–642. DOI:10.1049/iet-epa.2012.0338
- [6] Keskes H, Braham A. Recursive undecimated wavelet packet transform and DAG SVM for induction motor diagnosis. *IEEE Trans Ind Informatics.* 2015 Oct;11(5):1059–1066. DOI:10.1109/TII.2015.2462315
- [7] Mohammed Beer Gamal K, Handa SS, Murthy MVR. A fault diagnostic method for monitoring induction motor; 2017. [cited 2020 Dec 3]. Available from: <http://ijesc.org/>
- [8] Ordaz-Moreno A, de Jesus Romero-Troncoso R, Vite-Frias JA, et al. Automatic online diagnosis algorithm for broken-bar detection on induction motors based on discrete wavelet transform for FPGA implementation. *IEEE Trans Ind Electron.* 2008 May;55(5):2193–2202. DOI:10.1109/TIE.2008.918613
- [9] Trujillo-Guajardo LA, Rodriguez-Maldonado J, Moonem MA, et al. A multiresolution taylor-kalman approach for broken rotor bar detection in cage induction motors. *IEEE Trans Instrum Meas.* 2018 Jun;67(6):1317–1328. DOI:10.1109/TIM.2018.2795895
- [10] Kim H, Bin Lee S, Park S, et al. Reliable detection of rotor faults under the influence of low-frequency load torque oscillations for applications with speed reduction couplings. *IEEE Trans Ind Appl.* 2016 Mar;52(2):1460–1468. DOI:10.1109/TIA.2015.2508423
- [11] Kim YH, Youn YW, Hwang DH, et al. High-resolution parameter estimation method to identify broken rotor bar faults in induction motors. *IEEE Trans Ind Electron.* 2013;60(9):4103–4117. DOI:10.1109/TIE.2012.2227912
- [12] Liang X. Condition monitoring techniques for induction motors. In: 2017 IEEE Industry Applications Society Annual Meeting, IAS 2017; 2017 Nov; Janua; Vol. 2017. p. 1–10. DOI:10.1109/IAS.2017.8101860
- [13] Morinigo-Sotelo D, Romero-Troncoso RD, Panagiotou PA, et al. Reliable detection of rotor bars breakage in induction motors via MUSIC and ZSC. *IEEE Trans Ind Appl.* 2018 Mar;54(2):1224–1234. DOI:10.1109/TIA.2017.2764846

- [14] Liang X. Temperature estimation and vibration monitoring for induction motors and the potential application in electrical submersible motors. *Can J Electr Comput Eng.* 2019 Jun;42(3):148–162. DOI:10.1109/CJECE.2018.2875111
- [15] Janssens O, Schulz R, Slavkovikj V, et al. Thermal image based fault diagnosis for rotating machinery. *Infrared Phys Technol.* 2015 Nov;73:78–87. DOI:10.1016/j.infrared.2015.09.004
- [16] Sangeetha PB, Hemamalini S. Rational-dilation wavelet transform based torque estimation from acoustic signals for fault diagnosis in a three-phase induction motor. *IEEE Trans Ind Informatics.* 2019 Jun;15(6):3492–3501. DOI:10.1109/TII.2018.2874463
- [17] Frosini L, Harlisca C, Szabo L. Induction machine bearing fault detection by means of statistical processing of the stray flux measurement. *IEEE Trans Ind Electron.* 2015 Mar;62(3):1846–1854. DOI:10.1109/TIE.2014.2361115
- [18] Seshadrinath J, Singh B, Panigrahi BK. Investigation of vibration signatures for multiple fault diagnosis in variable frequency drives using complex wavelets. *IEEE Trans Power Electron.* 2014;29(2):936–945. DOI:10.1109/TPEL.2013.2257869
- [19] Picazo-Ródenas MJ, Antonino-Daviu J, Climente-Alarcon V, et al. Combination of noninvasive approaches for general assessment of induction motors. *IEEE Trans Ind Appl.* 2015 May;51(3):2172–2180. DOI:10.1109/TIA.2014.2382880
- [20] Sabouri M, Ojaghi M, Faiz J, et al. Model-based unified technique for identifying severities of stator inter-turn and rotor broken bar faults in SCIMs. *IET Electr Power Appl.* 2020 Feb;14(2):204–211. DOI:10.1049/iet-epa.2019.0267
- [21] Asad B, Vaimann T, Kallaste A, et al. Winding function based analytical model of squirrel cage induction motor for fault diagnostics. 2019 Mar. DOI:10.1109/IWED.2019.8664314
- [22] Reljić D, Jerkan D, Kanović Ž. Broken rotor bar fault detection using advanced im model and artificial intelligence approach. 2019 Jul. DOI:10.1109/EUROCON.2019.8861767
- [23] Edomwandekhoe K, Liang X. Advanced feature selection for broken rotor bar faults in induction motors. In: Conference Record – Industrial and Commercial Power Systems Technical Conference; 2018 May; Vol. 2018. p. 1–10. DOI:10.1109/ICPS.2018.8369981
- [24] Lee YO, Jo J, Hwang J. Application of deep neural network and generative adversarial network to industrial maintenance: a case study of induction motor fault detection. In: Proceedings – 2017 IEEE International Conference on Big Data, Big Data 2017; 2017 Jul; Janua; Vol. 2018. p. 3248–3253. DOI:10.1109/BigData.2017.8258307
- [25] Ferrucho-Alvarez ER, Cabal-Yepez E, Ledesma-Carrillo LM, et al. Broken rotor bar detection by image texture features and fuzzy logic. In: IECON Proceedings (Industrial Electronics Conference); Oct. 2019; Vol. 2019. p. 934–938. DOI:10.1109/IECON.2019.8927407
- [26] Noureddine L, Hafaifa A, Kouzou A. Fuzzy logic system for BRB defect diagnosis of SCIG-based wind energy system. In: Proceedings of the 2018 International Conference on Applied Smart Systems, ICASS 2018; 2019 Nov. p. 1–6. DOI:10.1109/ICASS.2018.8652011
- [27] Martínez-Morales JD, Palacios-Hernández ER, Campos-Delgado DU. Multiple-fault diagnosis in induction motors through support vector machine classification at variable operating conditions. *Electr Eng.* 2018 Mar;100(1):59–73. DOI:10.1007/s00202-016-0487-x
- [28] Sharma A, Mathew L, Chatterji S, et al. Artificial intelligence-based fault diagnosis for condition monitoring of electric motors. *Int J Pattern Recognit Artif Intell.* 2020 May. DOI:10.1142/S0218001420590430
- [29] Wang P, Shi L, Zhang Y, et al. Broken rotor bar fault detection of induction motors using a joint algorithm of trust region and modified bare-bones particle swarm optimization. *Chinese J Mech Eng (English Ed).* 2019 Dec;32(10). DOI:10.1186/s10033-019-0325-y
- [30] Gangsar P, Tiwari R. Performance analysis of support vector machine and wavelet packet transform based fault diagnostics of induction motor at various operating conditions. *Mech Mac Sci.* 2019;61:32–42.
- [31] Aouabdi S, Taibi M, Bouras S, et al. Using multi-scale entropy and principal component analysis to monitor gears degradation via the motor current signature analysis. *Mech Syst Signal Process.* 2017 Jun;90:298–316. DOI:10.1016/j.ymsp.2016.12.027
- [32] Glowacz A. Fault diagnosis of single-phase induction motor based on acoustic signals. *Mech Syst Signal Process.* 2019 Feb;117:65–80. DOI:10.1016/j.ymsp.2018.07.044
- [33] Martin-Diaz I, Morinigo-Sotelo D, Duque-Perez O, et al. An experimental comparative evaluation of machine learning techniques for motor fault diagnosis under various operating conditions. *IEEE Trans Ind Appl.* 2018 May;54(3):2215–2224. DOI:10.1109/TIA.2018.2801863
- [34] Lopez-Ramirez M, Ledesma-Carrillo LM, Garcia-Guevara FM, et al. Automatic early broken-rotor-bar detection and classification using Otsu segmentation. *IEEE Access.* 2020;8:112624–112632. DOI:10.1109/ACCESS.2020.3002545
- [35] Asad B, Vaimann T, Belahcen A, et al. Modified winding function-based model of squirrel cage induction motor for fault diagnostics. *IET Electr Power Appl.* 2020;14(9):1722–1734. DOI:10.1049/iet-epa.2019.1002
- [36] Luong P, Wang W. Smart sensor-based synergistic analysis for rotor bar fault detection of induction motors. *IEEE/ASME Trans Mechatron.* 2020;25(2):1067–1075. DOI:10.1109/TMECH.2020.2970274
- [37] Puche-Panadero R, Martinez-Roman J, Sapena-Bano A, et al. Diagnosis of rotor asymmetries faults in induction machines using the rectified stator current. *IEEE Trans Energy Convers.* 2020;35(1):213–221. DOI:10.1109/TEC.2019.2951008
- [38] Garcia-Calva TA, Morinigo-Sotelo D, Garcia-Perez A, et al. Demodulation technique for broken rotor bar detection in inverter-fed induction motor under non-stationary conditions. *IEEE Trans Energy Convers.* 2019;34(3):1496–1503. DOI:10.1109/tec.2019.2917405
- [39] Iglesias-Martinez ME, De Cordoba PF, Antonino-Daviu JA, et al. Detection of nonadjacent rotor faults in induction motors via spectral subtraction and auto-correlation of stray flux signals. *IEEE Trans Ind Appl.* 2019;55(5):4585–4594. DOI:10.1109/TIA.2019.2917861
- [40] Koti HN, Chen H, Sun Y, et al. On shortening the numerical transient in time-stepping finite element analysis of induction motors under static and dynamic eccentricity faults. In: IEEE Energy Convers. Congr. Expo. ECCE 2019; 2019. p. 3088–3095. DOI:10.1109/ECCE.2019.8913269
- [41] Panagiotou PA, Arvanitakis I, Lophitis N, et al. A new approach for broken rotor bar detection in induction motors using frequency extraction in stray flux

- signals. *IEEE Trans Ind Appl.* 2019;55(4):3501–3511. DOI:10.1109/TIA.2019.2905803
- [42] Park Y, Yang C, Kim J, et al. Stray flux monitoring for reliable detection of rotor faults under the influence of rotor axial air ducts. *IEEE Trans Ind Electron.* 2019;66(10):7561–7570. DOI:10.1109/TIE.2018.2880670
- [43] Soleimani Y, Cruz SMA, Haghjoo F. Broken rotor bar detection in induction motors based on air-gap rotational magnetic field measurement. *IEEE Trans Instrum Meas.* 2019. DOI:10.1109/TIM.2018.2870265
- [44] Didier G, Razik H, Rezzoug A. An induction motor model including the first space harmonics for broken rotor bar diagnosis. *Eur Trans Electr Power.* 2005 May;15(3):229–243. DOI:10.1002/etep.55
- [45] Pusca R, Romary R, Ceban A, et al. An online universal diagnosis procedure using two external flux sensors applied to the AC electrical rotating machines. *Sensors (Switzerland).* 2010 Nov;10(11):10448–10466. DOI:10.3390/s101110448
- [46] Mehrjou MR, Mariun N, Hamiruce Marhaban M, et al. Rotor fault condition monitoring techniques for squirrel-cage induction machine – a review. *Mech Syst Signal Process.* 2011 Nov;25(8):2827–2848. DOI:10.1016/j.ymsp.2011.05.007
- [47] Antonino-Daviu JA, Riera-Guasp M, Folch JR, et al. Validation of a new method for the diagnosis of rotor bar failures via wavelet transform in industrial induction machines. *IEEE Trans Ind Appl.* 2006 Jul;42(4):990–996. DOI:10.1109/TIA.2006.876082
- [48] Ali MZ, Shabbir MNSK, Liang X, et al. Machine learning-based fault diagnosis for single- and multi-faults in induction motors using measured stator currents and vibration signals. *IEEE Trans Ind Appl.* May 2019;55(3):2378–2391. DOI:10.1109/TIA.2019.2895797
- [49] Ali MZ, Shabbir MNSK, Zaman SMK, et al. Single- and multi-fault diagnosis using machine learning for variable frequency drive-fed induction motors. *IEEE Trans Ind Appl.* 2020 May;56(3):2324–2337. DOI:10.1109/TIA.2020.2974151
- [50] Silva DA, Silva JP, Rocha Neto AR. Novel approaches using evolutionary computation for sparse least square support vector machines. *Neurocomputing.* 2015 Nov;168:908–916. DOI:10.1016/j.neucom.2015.05.034
- [51] Long B, Xian W, Li M, et al. Improved diagnostics for the incipient faults in analog circuits using LSSVM based on PSO algorithm with mahalanobis distance. *Neurocomputing.* 2014 Jun;133:237–248. DOI:10.1016/j.neucom.2013.11.012
- [52] Zarei J. Induction motors bearing fault detection using pattern recognition techniques. *Expert Syst Appl.* 2012 Jan;39(1):68–73. DOI:10.1016/j.eswa.2011.06.042